High-Magnetic-Field-Induced First-Order Magnetic Transition and Tricritical Phenomenon in Antiferromagnetic Semimetal NdSb

Jun Zhao(赵俊)[1,2], Azizur Rahman(何安曼)[3], Wei Liu(刘威)[4], Langsheng Ling(凌浪生)[2], Yuyan Han(韩玉岩)[2], Chuanying Xi(郗传英)[2], Li Pi(皮雳)[2,5], Zhe Qu(屈哲)[2], Hao Gao(高浩)[1], and Lei Zhang(张蕾)[2*]

[1]*School of Mechanical and Electrical Engineering, Sanming University, Sanming 365004, China*
[2]*Anhui Key Laboratory of Low-Energy Quantum Materials and Devices, High Magnetic Field Laboratory, Hefei Institutes of Physical Science, Chinese Academy of Sciences, Hefei 230031, China*
[3]*Department of Physics, Lab of Low-dimensional Magnetism and Spintronic Devices, School of Physics, Hefei University of Technology, Hefei 230009, China*
[4]*Institutes of Physical Science and Information Technology, Anhui University, Hefei 230601, China*
[5]*Hefei National Research Center for Physical Sciences at Microscale, University of Science and Technology of China, Hefei 230026, China*

(Received 3 December 2024; accepted manuscript online 20 January 2025)

The antiferromagnetic (AFM) semimetal NdSb is well known for the interplay between its exotic magnetism and topological properties. However, its magnetism remains poorly understood. In this study, we thoroughly investigated the magnetization of NdSb single crystals with a high magnetic field (H) of up to 30 T applied in various directions. We found that the AFM phase is suppressed by a magnetic field of 9.41 T when $H \parallel [100]$ and 11.25 T when $H \parallel [110]$, whereas the suppression field ranges from 9.41 to 10.67 T with a hysteresis of 1.26 T when $H \parallel [111]$. The magnetization of $H \parallel [100]$, which is an easy direction with a typical magnetic transition, was studied in detail. The AFM phase with $H \parallel [100]$ was suppressed at lower temperatures, disappearing at approximately 6.25 K. The critical exponents $\beta = 0.234(3)$, $\gamma = 0.824(6)$, and $\delta = 4.90(6)$ were obtained for $H \parallel [100]$, and aligned with a tricritical mean-field model. Analysis of the critical behavior suggests a field-induced tricritical phenomenon for $H \parallel [100]$. An H–T phase diagram for an NdSb single crystal was constructed for $H \parallel [100]$, revealing a field-induced first-order transition and a tricritical point (TCP) at $T_{\rm tr} = 6.25$ K and $H_{\rm tr} = 9.41$ T. The clarification of the multiple magnetic phases and transitions in NdSb provides crucial insights into the correlation between its magnetism and topology.

DOI: 10.1088/0256-307X/42/2/027402 CSTR: 32039.14.0256-307X.42.2.027402

Rare-earth monopnictides (RePn: Re = rare earth, Pn = pnictogen) have generated immense interest from both scientific and technological perspectives owing to their exotic and exceptional properties, such as heavy-fermion behavior, unprecedentedly large magnetoresistance (MR), and topological phenomena.[1–9] For example, angle-resolved photoelectron spectroscopy (ARPES) and first-principles calculations have suggested the existence of topologically nontrivial surface states in LaBi.[10] Further, ARPES has revealed unconventional surface states in the antiferromagnetic (AFM) phase of NdBi.[1] Consequently, RePns are considered to be a crucial platform for studying the interplay between chirality, magnetism, and topology.[11] In particular, the AFM ordering observed in ReSb (Re = La, Ce, Pr, Sm, or Gd) highlights the correlation between magnetism and topology in this family.[5,7,12,13] For example, CeSb has been reported to undergo reconstruction of the bulk band structure and Fermi surface across the Néel temperature ($T_{\rm N}$), which is associated with p–f mixing.[14] Moreover, magnetic Weyl points have been proposed in the ferromagnetic (FM) phase of CeSb under an external magnetic field.[12]

In the monopnictide RePn family, AFM semimetal NdSb stands out because of its various magnetically ordered phases and excellent properties. NdSb has a NaCl-type crystal structure with cubic symmetry and belongs to the space group $Fm\bar{3}m$ (No. 225).[15,16] An extremely large MR of approximately 400% and field-induced metamagnetic transitions have been observed in this material, suggesting the potential for new functionalities that combine topological characteristics with electronic correlations.[5,17] In addition, a Dirac-like semimetal state and field-induced reconstruction of the Fermi surface have been revealed in this material,[18,19] which are associated with $\mathcal{PT}$-(space-inversion and time-reversal) symmetry breaking.[20] Furthermore, a complex evolution of the electronic structure across magnetic transitions has been observed in NdSb.[21] ARPES measurements and first-principles calculations have indicated that the possible unconventional $2q$ AFM order in NdSb can induce unusual modulations in its electronic structure.[22] Moreover, a pressure-induced structural transition from the

*Corresponding author. Email: zhanglei@hmfl.ac.cn
© 2025 Chinese Physical Society and IOP Publishing Ltd. All rights, including for text and data mining, AI training, and similar technologies, are reserved.

$Fm\bar{3}m$ phase to the $P4/mmm$ phase occurs at a P_C of approximately 18 GPa, resulting in a yurt-shaped evolution in response to the magnetic field, pressure, and temperature.[23]

However, the correlation between the magnetism and topological properties of NdSb lacks detailed clarification, particularly regarding the anisotropic magnetism and direction-dependent transitions. In this study, we conducted a thorough investigation of the magnetization of NdSb single crystals under a high magnetic field (H) of up to 30 T. AFM transitions at a T_N of approximately 15 K were observed for all field directions, which were suppressed by a magnetic field of 9.41 T when $H \parallel [100]$ and 11.25 T when $H \parallel [110]$. However, the suppression field ranged from 9.41 to 10.67 T with a hysteresis of 1.26 T when $H \parallel [111]$. Magnetization with $H \parallel [100]$ and typical magnetic characteristics was studied in detail. The AFM phase for $H \parallel [100]$ was suppressed by the external magnetic field, shifted toward lower temperatures, and disappeared at approximately 6.25 K. Reliable critical exponents (β, γ, and δ) were obtained near the critical point, revealing field-induced tricritical behavior in this system. Furthermore, an H–T phase diagram for NdSb single crystals was constructed for $H \parallel [100]$, in which a field-induced first-order transition from AFM to forced FM was identified. Additionally, a tricritical point (TCP) at $T_{tr} = 6.25$ K and $H_{tr} = 9.41$ T was determined.

The sample synthesis, characterization, and experimental details are included in the Supplementary Material. Figures 1(a), 1(b), and 1(c) depict the temperature-dependent magnetization [$M(T)$] of NdSb single crystals with the magnetic field (H) applied along the [100] ($H \parallel [100]$), [110] ($H \parallel [110]$), and [111] ($H \parallel [111]$) directions, respectively. The $M(T)$ curves were measured under $H = 1$ kOe conditions using zero-field-cooling (ZFC) and field-cooling (FC) sequences; the measurement configuration is illustrated in the inset of Fig. 1(d). A sharp peak appeared in each $M(T)$ curve as the temperature decreased, with no divergence between the ZFC and FC $M(T)$ curves. The sharp decline at low temperatures and the coincidence of the ZFC and FC $M(T)$ curves are typical features of AFM transitions, indicating an AFM ground state in NdSb.[18] The AFM phase transition is further indicated by peaks in the temperature-dependent resistivity and specific heat.[5,17] The Néel temperatures were determined from the peaks as approximately $T_N = 14.81$ K for $H \parallel [100]$, 15.03 K for $H \parallel [110]$, and 15.10 K for $H \parallel [111]$, consistently at approximately 15 K. The reciprocal susceptibility [$\chi^{-1}(T) = H/M$] curves are plotted on the right axis in Figs. 1(a), 1(b), and 1(c). Above T_N, $\chi^{-1}(T)$ exhibits linear behavior, which is fitted with the Curie–Weiss law [$\chi = C/(T - \Theta_{CW})$] (where C is the Curie constant and Θ_{CW} is the Curie–Weiss temperature). From this fitting, $\Theta_{CW} = -3.30$ K for $H \parallel [100]$, -0.99 K for $H \parallel [110]$, and -1.10 K for $H \parallel [111]$. These negative Θ_{CW} values indicate AFM coupling, which is consistent with the observed AFM ground state in NdSb. Figure 1(d) shows the field-dependent magnetization [$M(H)$] at $T = 2$ K for $H \parallel [100]$, $H \parallel [110]$, and $H \parallel [111]$. As H increases, all $M(H)$ curves increase slowly at low fields, followed by abrupt steps. For $H \parallel [100]$, the step is located at approximately $H_C^{[100]} = 94.1$ kOe (9.41 T). The saturation magnetization M_{sat} was estimated to be approximately 3.123(2) μ_B/(f.u.) at $T = 2$ K for $H \parallel [100]$, which is smaller than the theoretical value of 3.87 μ_B for Nd^{3+}. For $H \parallel [110]$ and $H \parallel [111]$, a gentler step-like behavior is exhibited at $H_C^{[110]} \sim 112.5$ kOe (11.25 T) and $H_C^{[111]} \sim 94.1$ kOe (9.41 T), respectively. A magnetic hysteresis of $\Delta H = 1.26$ T occurs for $H \parallel [111]$, indicating a field-induced first-order phase transition. The saturation magnetization M_{sat} for $H \parallel [110]$ was almost the same as that for $H \parallel [111]$, which was estimated to be approximately 2.271(4) μ_B/(f.u.) at $T = 2$ K, which is smaller than that for $H \parallel [100]$.

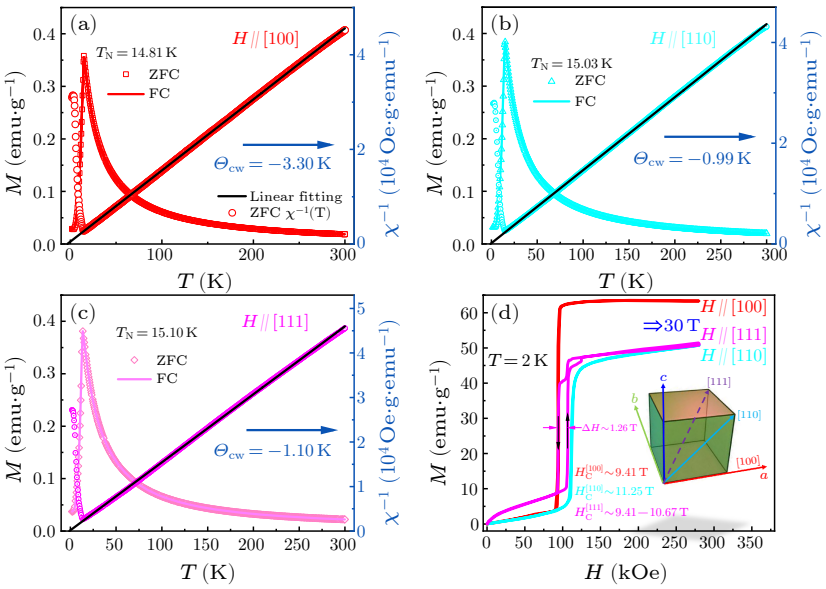

Fig. 1. Temperature-dependent magnetization [$M(T)$] and reciprocal of susceptibility [$\chi^{-1}(T)$] of NdSb single crystals with $H = 1$ kOe for (a) $H \parallel [100]$, (b) $H \parallel [110]$, and (c) $H \parallel [111]$. (d) Field-dependent magnetization [$M(H)$] up to 30 T at 2 K for $H \parallel [100]$, $H \parallel [110]$, and $H \parallel [111]$ (the inset gives the measurement configuration).

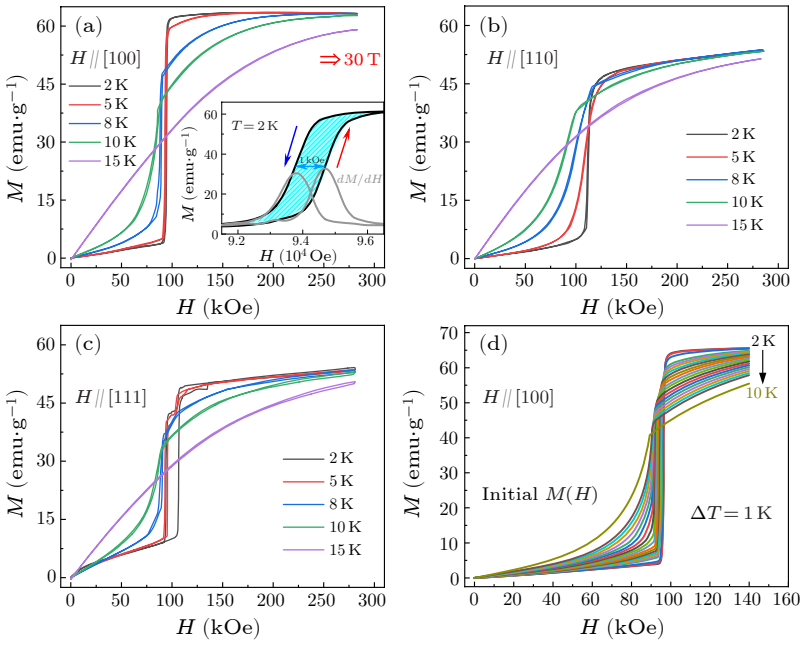

Fig. 2. Field-dependent magnetization $M(H)$ curves at selected temperatures up to 30 T for (a) $H \parallel [100]$, (b) $H \parallel [110]$, and (c) $H \parallel [111]$ (the inset shows the enlarged $M(H)$ at $T = 2$ K with a magnetic hysteresis for $H \parallel [100]$). (d) Initial $M(H)$ around the critical temperature T_C for $H \parallel [100]$.

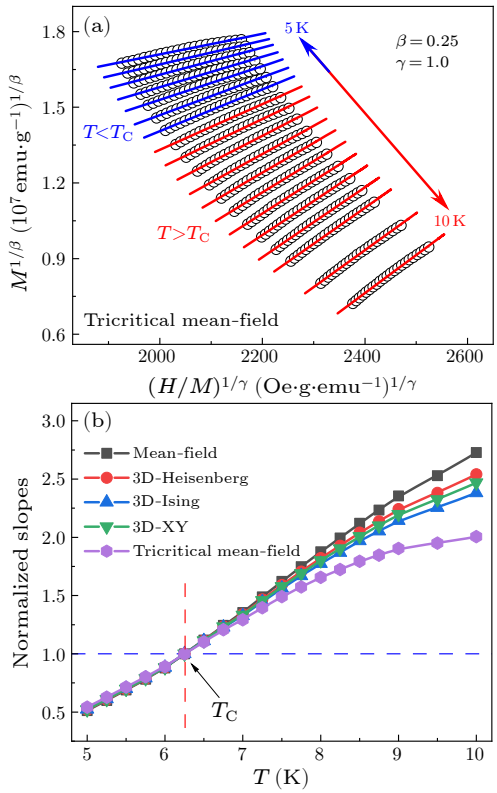

Fig. 3. (a) Modified Arrott plot (MAP) of $M^{1/\beta}$ versus $(H/M)^{1/\gamma}$ for $H \parallel [100]$ based on the tricrtical mean-field model. (b) Normalized slope (NS) as a function of temperature for different models.

Figures 2(a), 2(b), and 2(c) show the $M(H)$ curves at temperatures of up to 30 T for $H \parallel [100]$, $H \parallel [110]$, and $H \parallel [111]$, respectively. As the temperature increases, the step behaviors become gentler and eventually vanish for the $M(H)$ curve at $T = 15$ K. The inset of Fig. 2(a) presents an enlarged $M(H)$ and dM/dH at $T = 2$ K for $H \parallel [100]$, which reveals a magnetic hysteresis of $\Delta H = 1000$ Oe, significantly smaller than that for $H \parallel [111]$. These field-induced phase transitions have also been confirmed by other measurements such as MR and specific heat.[5,17] For an in-depth investigation of the field-induced phase transition, the magnetization for $H \parallel [100]$, which is the easiest direction and associated with typical magnetism, was studied in detail. The initial isothermal $M(H)$ curves near the critical temperature T_C for $H \parallel [100]$ are shown in Fig. 2(d) for a critical analysis. For a magnetic phase transition, the $M(H)$ curves in the vicinity of the phase transition generally adhere to the Arrott–Noakes equations of state:[24]

$$(H/M)^{1/\gamma} = (T - T_C)/T_C + (M/M_1)^{1/\beta}, \qquad (1)$$

where M_1 is a constant, T_C represents the critical temperature, and γ and β are the critical exponents. A plot of $M^{1/\beta}$ versus $(H/M)^{1/\gamma}$, known as the modified Arrott plot (MAP), should consist of a set of parallel straight lines in the high-field region, with the line at T_C intersecting the origin. The Banerjee criterion states that the positive and negative slopes of these lines indicate whether the phase transition is of the second-order (continuous) or first-order (discontinuous) type.[24–26] Several theoretical models have been adopted to establish an appropriate MAP for NdSb. Considering the three-dimensional (3D) cubic symmetry, the spatial dimensionality (d) is regarded as $d = 3$. Consequently, theoretical models within the framework of $d = 3$ are preferred. MAPs based on the 3D-Heisenberg ($\beta = 0.365$, $\gamma = 1.386$), 3D-Ising ($\beta = 0.325$, $\gamma = 1.240$), 3D-XY ($\beta = 0.345$, $\gamma = 1.316$), and tricritical mean-field ($\beta = 0.25$, $\gamma = 1.0$) models were employed[27,28] (See Fig. S3). The MAP based on the tricritical mean field, as shown in Fig. 3(a), exhibits a set of straight lines

in the high-field region, which is more appropriate than the other models. To determine the best model for NdSb, the normalized slope (NS) was used, which is defined as $NS = S(T)/S(T_C)$, where $S(T)$ represents the slope of $M^{1/\beta}$ versus $(H/M)^{1/\gamma}$. The best model will have the NS closest to '1'.[29,30] Figure 3(b) presents NS as a function of temperature, showing that the NS for the tricritical mean-field model is closest to '1'. This confirms that the tricritical mean-field model is the most suitable for elucidating magnetic interactions in NdSb.

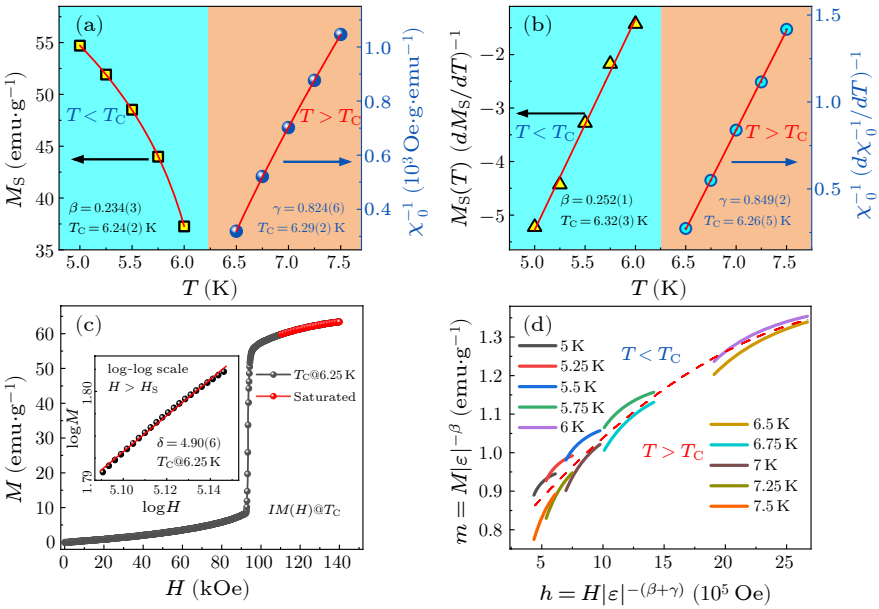

Fig. 4. (a) M_S (left) and χ_0^{-1} (right) as a function of temperature with fitting curves (red). (b) Kouvel–Fisher (KF) plot for $M_S(T)/[dM_S(T)/dT]$ (left) and $\chi_0^{-1}/[d\chi_0^{-1}(T)/dT]$ (right) with linear fitting lines. (c) Fitting of initial $M(H)$ at $T_C = 6.25$ K and a log–log plot in the inset. (d) Scaling plot of renormalized magnetization versus renormalized field $[m(h)]$ for $H \parallel [100]$.

Nevertheless, the precise critical exponents must be strictly determined. In this study, a rigorous iterative procedure was adopted. The critical exponent β corresponds to the spontaneous magnetization M_S below T_C, γ is associated with the initial magnetic susceptibility χ_0^{-1} above T_C, and δ is related to the critical isotherm magnetization $M(H)$ at T_C. These critical exponents satisfy the following relationships:[31]

$$M_S(T) = M_0(-\varepsilon)^{\beta}, \quad \varepsilon < 0, \quad T < T_C, \tag{2}$$

$$\chi_0^{-1}(T) = (h_0/M_0)\varepsilon^{\gamma}, \quad \varepsilon > 0, \quad T > T_C, \tag{3}$$

$$M = DH^{1/\delta}, \quad \varepsilon = 0, \quad T = T_C, \tag{4}$$

where $\varepsilon = (T - T_C)/T_C$ represents the reduced temperature and h_0/M_0, M_0, and D are the critical amplitudes. According to the iteration method, $M_S(T)$ and $\chi_0^{-1}(T)$ were first obtained from the intercepts of the MAP based on the tricritical mean-field model, which is the best theoretical model for NdSb. Subsequently, a set of parameters was fitted using Eqs. (2) and (3) from $M_S(T)$ and $\chi_0^{-1}(T)$. Finally, another MAP was constructed based on the obtained parameters. This procedure was repeated until the values of β and γ stabilized. Figure 4(a) shows the final fits of $M_S(T)$ and $\chi_0^{-1}(T)$. The critical exponents $\beta = 0.234(3)$ with $T_C = 6.24(2)$ K and $\gamma = 0.824(6)$ with $T_C = 6.29(2)$ K were obtained. Further, the Kouvel–Fisher (KF) technique was also used to examine the critical exponents:[32]

$$\frac{M_S(T)}{dM_S(T)/dT} = \frac{T - T_C}{\beta}, \tag{5}$$

$$\frac{\chi_0^{-1}(T)}{d\chi_0^{-1}(T)/dT} = \frac{T - T_C}{\gamma}. \tag{6}$$

The (KF) technique indicated that $M_S(T)/[dM_S(T)/dT]$ and $\chi_0^{-1}(T)/[d\chi_0^{-1}(T)/dT]$ are linearly dependent on the temperature, with slopes of $1/\beta$ and $1/\gamma$, respectively. Using this method, we determined $\beta = 0.252(1)$ with $T_C = 6.32(3)$ K, and $\gamma = 0.849(2)$ with $T_C = 6.26(5)$ K, as shown in Fig. 4(b). The critical exponents obtained using the KF technique closely matched those derived from the iterative method, indicating the reliability of the results.

The critical exponent δ can be determined by fitting the isotherm $M(H)$ at T_C to Eq. (4) as shown in Fig. 4(c), with a log–log scale in the inset. Fitting $\log(M)$ over $\log(H)$ yields $\delta = 4.90(6)$. The independently obtained critical exponents were inherently correlated using the Widom scaling law:[33]

$$\delta = 1 + \frac{\gamma}{\beta}. \tag{7}$$

Using values from the iteration method and the KF technique, we calculated $\delta = 4.519(4)$ and $\delta = 4.368(5)$, which confirm the reliability and self-consistency of the obtained critical exponents.

Furthermore, according to the universality principle of phase transitions, $M(H)$ near the critical temperature can be scaled using the scaling equation.[26] The renormalized magnetization is defined as $m \equiv \varepsilon^{-\beta}M(H, \varepsilon)$ and the renormalized field as $h \equiv H\varepsilon^{-(\beta+\gamma)}$. The scaling equation

is expressed as

$$m = f_{\pm}(h), \tag{8}$$

where f represents a regular function with f_+ for $T > T_C$ and f_- for $T < T_C$. The initial $M(H)$ curves around T_C were rescaled according to Eq. (8), and collapse into two independent branches above and below T_C, as shown in Fig. 4(d). The scaling equations, along with the Widom scaling law, confirmed the validity of the method and reliability of the obtained exponents.

Table 1. Critical exponents of NdSb, along with related materials and different theoretical models (MAP: modified Arrott plot; KF: Kouvel–Fisher technique; CI: Critical isotherms).

Composition	Technique	Ref.	T_C	β	γ	δ
NdSb ($H \parallel [100]$)	This work	MAP	6.24(2)	0.234(3)	0.824(6)	–
		KF	6.32(3)	0.252(1)	0.849(2)	–
		CI	6.25			4.90(6)
DySb	Experiment	[34]	7.5	0.244(2)	0.827(2)	4.425(1)
DyBi	Experiment	[35]	8.75	0.234(8)	0.904(3)	5.03(2)
Tricritical mean field	Theory	[27]	–	0.25	1.0	5.0
3D-Ising	Theory	[28]	–	0.325	1.24	4.82
3D-XY	Theory	[28]	–	0.346	1.316	4.81
3D-Heisenberg	Theory	[28]	–	0.365	1.386	4.8
Mean-field	Theory	[28]	–	0.5	1.0	3.0

Table 1 lists the critical exponents of NdSb single crystals along with those of related materials and various theoretical models. The critical exponents of NdSb single crystals approximate those predicted by the tricritical mean-field model and are similar to those of DySb and DyBi. In a homogeneous magnet, the universality class is determined by the exchange distance between the spins, denoted by $J(r)$. According to renormalization group theory, $J(r)$ decreases with spatial distance r, where $J(r) \approx r^{-(d+\sigma)}$ for long-range interactions and $J(r) \approx e^{-r/b}$ for short-range interactions (where σ is the critical exponent associated with the exchange distance and b is the spatial scaling factor).[31,36] The relationship between γ and σ can be expressed as[31,36]

$$\gamma = 1 + \frac{4}{d}\frac{n+2}{n+8}\Delta\sigma + \frac{8(n+2)(n-4)}{d^2(n+8)^2} \times \left[1 + \frac{2G(\frac{d}{2})(7n+20)}{(n-4)(n+8)}\right]\Delta\sigma^2, \tag{9}$$

where $\Delta\sigma = \sigma - \frac{d}{2}$ and $G(\frac{d}{2}) = 3 - \frac{1}{4}(\frac{d}{2})^2$. When $\sigma > 2$, the Heisenberg model with short-range magnetic exchange is applicable, making $J(r)$ decrease more rapidly than r^{-5}.[36] Conversely, when $\sigma < 3/2$, the mean-field model with long-range magnetic exchange is valid, leading to $J(r)$ decreasing more slowly than $r^{-4.5}$.[36] In the present case, with $\gamma = 0.824(6)$ and $d = 3$, we calculated $\sigma = 1.701(8)$ for NdSb, which falls between the long- and short-range interactions ($3/2 < \sigma < 2$). This implies that $J(r)$ decays as $J(r) \approx r^{-4.7}$.

The tricritical mean-field model indicates tricritical behavior, which is typically characterized by multiple phases modulated by external variables, such as temperature, field, and pressure. Therefore, constructing the phase diagram to clarify the various magnetic phases and transitions is necessary. The phase transition affects the slopes of the MAP, which can distinguish the boundaries between different phases.[34] Figure 5(a) displays the MAP on a log–log scale. In the high-field region, the MAP of NdSb exhibits a set of straight lines, as shown in the inset of Fig. 5(a). However, in the low-field region, the curves deviate from a linear relationship because of the occurrence of phase transitions. In the field region $H_{AF} < H < H_S$, the curves exhibit negative slopes, indicating a first-order transition according to the Banerjee criterion.[24–26] Two distinct turning points corresponding to H_{AF} and H_S can be identified. Figure 5(b) shows the $M(T)$ curves for different magnetic fields with $H \parallel [100]$. The AFM phase was suppressed when a higher magnetic field was applied, from which the T_N was extracted.

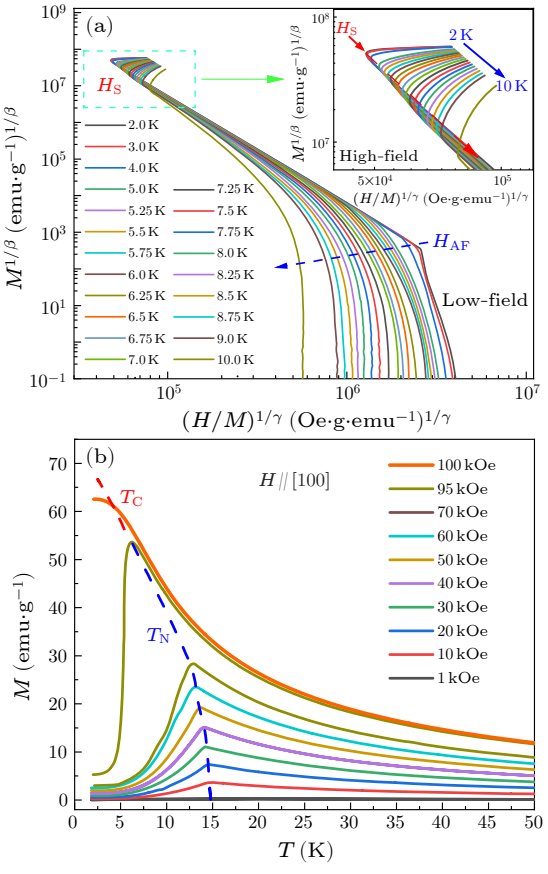

Fig. 5. (a) MAP in low-field region on a log–log scale for $H \parallel [100]$ (the inset is the magnification). (b) $M(T)$ curves under different fields for $H \parallel [100]$.

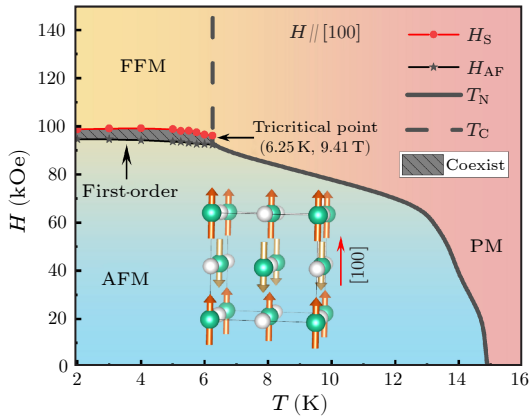

Fig. 6. (a) H–T phase diagram for NdSb single crystals with $H \parallel [100]$ (PM, AFM, and FFM represent paramagnetic, antiferromagnetic, and forced ferromagnetic states, respectively).

Based on Figs. 5(a) and 5(b), a detailed H–T phase diagram for NdSb single crystals with $H \parallel [100]$ was constructed, as shown in Fig. 6. The H–T phase diagram clearly distinguishes multiple phases of NdSb, including antiferromagnetic (AFM), forced ferromagnetic (FFM), and paramagnetic (PM) phases. NdSb exhibits an A-type AFM ground state below $T_N \sim 15$ K, similar to that of NdBi.[1] In contrast to other rare-earth monopnictides, such as DySb and DyBi,[34,35] NdSb and NdBi display only one AFM phase, as illustrated in the inset of Fig. 6. The H–T phase diagram shows that the AFM phase was suppressed by the external field and disappeared at approximately 6.25 K. As the field increased, the AFM phase was polarized to an FFM state at a field of 9.4 T.[20] The magnetic transition from AFM to FFM is of the first-order type, as supported by the negative slope of the MAP and magnetic hysteresis.[18] A tricritical point (TCP) is located at the endpoint of the first-order phase-transition boundary ($T_{tr} = 6.25$ K, $H_{tr} = 9.41$ T). A region of coexistence occurs between the AFM and FFM phases. The three phases, i.e., AFM, PM, and FFM, converge at the TCP, which serves as an intricate balance point. At the TCP, exotic physical phenomena are expected owing to strong fluctuations from different phases, such as topological states, spin flips, and quantum phase transitions.[37] In NdSb, a tip appears on the resistivity curve, and a peak emerges on the heat capacity curve at the TCP, indicating enhanced spin scattering at this point.[5] The modulation of AFM ordering significantly impacts the $\mathcal{PT}$-(space-inversion and time-reversal) symmetry breaking at the surface, leading to band folding.[20] Moreover, the presence of distinct domains yields different electronic structures at the surface, corresponding to various orientations of the magnetic moments in the AFM state relative to the surface.[38] Therefore, tuning the behaviors around the TCP is crucial for NdSb. These results pave the way for understanding the relationship between the magnetism and topological properties of this system.

In summary, the anisotropic magnetization of NdSb single crystals was systematically investigated with a magnetic field (H) applied in various crystal directions. As the temperature decreased, AFM transitions occurred at approximately $T_N = 15$ K. However, the AFM phase was suppressed by applied magnetic fields of $H = 9.41$ T when $H \parallel [100]$ and $H = 11.25$ T when $H \parallel [110]$, whereas the suppression field ranged from 9.41 to 10.67 T with a hysteresis of 1.26 T when $H \parallel [111]$. Magnetization with $H \parallel [100]$ and typical magnetic characteristics was studied in detail. The AFM phase of $H \parallel [100]$ was suppressed by an external magnetic field and disappeared at approximately 6.25 K. The critical exponents $\beta = 0.234(3)$, $\gamma = 0.824(6)$, and $\delta = 4.90(6)$ were obtained for $H \parallel [100]$ around T_C, as examined using the Kouvel–Fisher (KF) technique and Widom scaling law. These critical exponents aligned with the tricritical mean-field model, indicating field-induced tricritical behavior. An H–T phase diagram with $H \parallel [100]$ for NdSb single crystals was constructed. A field-induced first-order magnetic transition from AFM to FFM was observed, and a TCP at $T_{tr} = 6.25$ K and $H_{tr} = 9.41$ T was identified at the intersection of the AFM, FFM, and PM phases. Clarification of the magnetism of NdSb single crystals enhances our understanding of the correlation between magnetism and topology.

Acknowledgements. This work was supported by the National Key R&D Program of China (Grant No. 2024YFA1611103), the National Natural Science Foundation of China (Grant Nos. 12374128, 12374129, 12074386, 11974181, 12204006, and 12250410238), the Fujian Natural Science Foundation Project (Grant No. 2024J08082), the Foundation for the Introduction of High-Level Talents and the Scientific Research Launch Project of Sanming University (Grant No. 113/KD23016P), Fujian Key Technology Innovation Projects (University Category) (Grant No. 2022G02010), the Anhui Provincial Major S&T Project (Grant No. 202305a12020005), and the Alliance of International Science Organizations (Grant Nos. ANSO-VF-2022-03 and ANSO-VF-2023-03). A portion of this work was supported by the Basic Research Program of the Chinese Academy of Sciences Based on Major Scientific Infrastructures (Grant No. JZHKYPT-2021-08) and the High Magnetic Field Laboratory of Anhui Province under Contract No. AHHM-FX-2020-02. We thank the Steady High Magnetic Field Facility (https://cstr.cn/31125.02.SHMFF.XRD and (https://cstr.cn/31125.02.SHMFF.WM2) of CAS for data collection and analysis.

References

[1] Schrunk B, Kushnirenko Y, Kuthanazhi B, Ahn J, Wang L L *et al.* 2022 *Nature* **603** 610
[2] Zeng L K, Lou R, Wu D S, Xu Q N *et al.* 2016 *Phys. Rev. Lett.* **117** 127204
[3] Niu X H, Xu D F, Bai Y H, Song Q, Shen X P *et al.* 2016 *Phys. Rev. B* **94** 165163
[4] Guo P J, Yang H C, Zhang B J, Liu K, and Lu Z Y 2016 *Phys. Rev. B* **93** 235142
[5] Wakeham N, Bauer E D, Neupane M, and Ronning F 2016 *Phys. Rev. B* **93** 205152
[6] Wu F, Guo C Y, Smidman M, Zhang J L, and Yuan H Q 2017 *Phys. Rev. B* **96** 125122
[7] Wu Y, Lee Y, Kong T, Mou D, Jiang R *et al.* 2017 *Phys. Rev. B* **96** 035134

[8] Petit L, Szotek Z, Lüders M, and Svane A 2016 *J. Phys.: Condens. Matter* **28** 223001
[9] Shekhar C, Nayak A K, Sun Y, Schmidt M, Nicklas M *et al.* 2015 *Nat. Phys.* **11** 645
[10] Nayak J, Wu S C, Kumar N, Shekhar C, Singh S *et al.* 2017 *Nat. Commun.* **8** 13942
[11] Matt C E, Liu Y, Pirie H, Drucker N C, Jo N H *et al.* 2022 *Phys. Rev. B* **105** 085134
[12] Guo C, Cao C, Smidman M, Wu F, Zhang Y, Steglich F, Zhang F C, and Yuan H 2017 *npj Quan. Mater.* **2** 39
[13] Duan C G, Sabirianov R F, Mei W N, Dowben P A, Jaswal S S, and Tsymbal E Y 2007 *J. Phys.: Condens. Matter* **19** 315220
[14] Kuroda K, Arai Y, Rezaei N, Kunisada S, Sakuragi S *et al.* 2020 *Nat. Common.* **11** 2888
[15] Wakabayashi N and Furrer A 1976 *Phys. Rev. B* **133** 4343
[16] Manfrinetti P, Provino A, Morozkin A V, and Isnard O 2009 *J. Alloys Compd.* **487** L28
[17] Zhou Y, Zhu X, Huang S, Chen X, Zhou Y, An C, Zhang B, Yuan Y, Xia Z, Gu C, and Yang Z 2017 *Phys. Rev. B* **96** 205122
[18] Wang Y, Yu J H, Wang Y Q, Xi C Y, Ling L S, Zhang S L, Wang J R, Xiong Y M, Han T, Han H *et al.* 2018 *Phys. Rev. B* **97** 115133
[19] Neupane M, Hosen M M, Belopolski I, Wakeham N, Dimitri K, Dhakal N, Zhu J X, Hasan M Z, Bauer E D, and Ronning F 2016 *J. Phys.: Condens. Matter* **28** 23LT02
[20] Honma A, Takane D, Souma S, Wang Y, Nakayama K, Kitamura M, Horiba K, Kumigashira H, Takahashi T, Ando Y, and Sato T 2023 *Phys. Rev. B* **108** 115118
[21] Sakhya A P, Wang B, Kabir F, Huang C Y, Hosen M M, Singh B, Regmi S, Dhakal G, Dimitri K, Sprague M *et al.* 2022 *Phys. Rev. B* **106** 235119
[22] Li P, Li T, Liao S, Cao Z, Xu R, Wang Y, Yao J, Cui S, Sun Z, Wang Y, Wan X, Jiang J, and Feng D 2023 *npj Quan. Mater.* **8** 22
[23] Zhou Y, Chen X, Zhou Y, Yu J, Zhu X, An C, Park C, Wan X, Yang X, and Yang Z 2022 *Sci. China-Phys. Mech. Astron.* **65** 288211
[24] Arrott A and Noakes J E 1967 *Phys. Rev. Lett.* **19** 786
[25] Banerjee B K 1964 *Phys. Lett.* **12** 16
[26] Zhang L 2018 *Acta Phys. Sin.* **67** 137501
[27] Huang K 1987 *Wiley* **2nd** 017202
[28] Kaul S N 1985 *J. Magn. Magn. Mater.* **53** 5
[29] Fan J, Ling L, Hong B, Zhang L, Pi L, and Zhang Y 2010 *Phys. Rev. B* **81** 144426
[30] Wang X Y, Lin J F, Zeng X Y, Wang H, Ma X P, Wang Y T, Han K, and Xia T L 2023 *Chin. Phys. Lett.* **40** 067503
[31] Fisher M E 1967 *Rep. Prog. Phys.* **30** 615
[32] Kouvel J S and Fisher M E 1964 *Phys. Rev.* **136** A1626
[33] Widom B and Chem J 1965 *Phys.* **43** 3898
[34] Liu W, Liang D, Meng F, Zhao J, Zhu W, Fan J, Pi L, Zhang C, Zhang L, and Zhang Y 2020 *Phys. Rev. B* **102** 174417
[35] Zhao J, Rahman A, Liu W, Meng F, Ling L, Han Y, Xi C, Tong W, Xu L, Tian Z, Pi L, Zhang L, and Zhang Y 2022 *Phys. Rev. B* **106** 224412
[36] Fisher M E, Ma S K, and Nickel B G 1972 *Phys. Rev. Lett.* **29** 917
[37] Du Z, Rahman A, Song J, Zhao J, Liu W, Fan J, Ma C, Ge M, Xiong Y, Pi L *et al.* 2023 *Sci. China-Phys. Mech. & Astron.* **66** 297511
[38] Kushnirenko Y, Kuthanazhi B, Wang L L, Schrunk B, O'Leary E, Eaton A, Canfield P C, and Kaminski A 2023 *Phys. Rev. B* **108** 115102